UDK 669.18
Original scientific article/Izvirni znanstveni članek

ISSN 1580-2949
MTAEC9, 46(4)361(2012)

THERMODYNAMIC ANALYSIS OF THE FORMATION OF NON-METALLIC INCLUSIONS DURING THE PRODUCTION OF C45 STEEL

TERMODINAMIČNA ANALIZA NASTANKA NEKOVINSKIH VKLJUČKOV PRI IZDELAVI JEKLA C45

Luka Krajnc[1], Grega Klančnik[2], Primož Mrvar[2], Jožef Medved[2]

[1]Štore Steel, d. o. o., Železarska 3, 3220 Štore, Slovenia
[2]University of Ljubljana, Faculty of Natural Science and Engineering, Department for Materials and Metallurgy, Aškerčeva 12, 1000 Ljubljana, Slovenia
luka.krajnc@store-steel.si

Prejem rokopisa – received: 2011-11-11; sprejem za objavo – accepted for publication: 2012-03-01

C45 steel belongs to the group of carbon steels and is used in the normalized and tempered states for heavily stressed parts in the automobile industry. Nowadays, a major problem in steelmaking is non-metallic inclusions, which can form during various steps of the steelmaking process and are detrimental to the mechanical properties of the steel.
In scope of this work we have tried to determine during which steps of the steelmaking process the non-metallic inclusions are formed. Samples were taken from three different steps of the steelmaking process, i.e., from the electric arc furnace, from the ladle furnace and from the tundish. The samples were then chemically analysed. The results were used for a thermodynamic simulation with Thermo-Calc. Other samples were prepared from another simultaneously taken probe and were partly subjected to differential scanning calorimetry (DSC) and partly metallographically prepared. Photographs were taken with a light microscope, from which the phase composition was calculated. The non-metallic inclusions in our samples were analysed with EDS – photographs were taken and point and mapping analyses were made on them.
We found that in our C45 steel sample, spinel ($MgO \cdot Al_2O_3$) and aluminate (Al_2O_3) inclusions can be found at the end of the ladle-furnace treatment. In the tundish sample only small aluminate and spinel inclusions and a lot of MnS inclusions were found.

Keywords: non-metallic inclusions, thermodynamics, C45 steel

Jeklo C45 je ogljikovo jeklo, ki se v normaliziranem in poboljšanem stanju uporablja za obremenjene dele v avtomobilski industriji. Slabše mehanske lastnosti in krajša uporabna doba pa so predvsem povezane z nekovinskimi vključki. Le-ti lahko nastanejo pri različnih stopnjah procesa izdelave jekla.
V okviru tega dela smo poskušali ugotoviti, pri katerih stopnjah procesa izdelave jekla nastanejo nekovinski vključki. V ta namen smo vzeli vzorce pri treh stopnjah izdelave jekla: na elektroobločni peči, na ponovčni peči in iz vmesne ponovce na napravi za kontinuirno litje jekla. Naredili smo kemično analizo vzorcev, ki smo jo uporabili za termodinamični ravnotežni izračun s programskim orodjem Thermo-Calc. Vzorce smo razrezali in naredili diferenčno vrstično kalorimetrijo (DSC), metalografsko pripravljene vzorce pa smo slikali s svetlobnim mikroskopom. Za kvalitativno metalografsko analizo smo uporabili program analySIS 5.0 in z njim ugotovili delež mikrostrukturnih sestavin. Vzorce smo pregledali in slikali še z vrstičnim elektronskim mikroskopom, naredili smo tudi točkovno analizo vključkov in določili porazdelitev elementov glede na površino.
Ugotovili smo, da so se v našem vzorcu jekla C45 pojavljali pri koncu obdelave na ponovčni peči špinelni ($MgO \cdot Al_2O_3$) in aluminatni (Al_2O_3) vključki, ki so neželeni, trdi in krhki vključki. Pri litju jekla na napravi za kontinuirno litje so se v našem vzorcu v jeklu pojavljali le majhni špinelni in aluminatni vključki, videli pa smo mnogo MnS-vključkov.

Ključne besede: nekovinski vključki, termodinamika, jeklo C45

1 INTRODUCTION

With the advances in technology, with the introduction of new secondary-steelmaking processes and with the increasingly higher quality demands from buyers, there has been, especially in recent years, a greater demand for better mechanical properties from steel. This can only be guaranteed, however, if we can control the quantity, size and distribution of the non-metallic inclusions in the steel.

The non-metallic inclusions in steel are formed from metal elements, such as iron, manganese, silicon, aluminium and calcium and non-metal elements such as oxygen, sulphur, nitrogen and phosphor. The non-metallic inclusions are divided in two groups, i.e., external and internal. The external inclusions are formed because the melt is in contact with slag and refractory and some parts of these two can be caught in the melt. These inclusions are large, with an irregular shape and they are detrimental to the mechanical properties of the steel. Internal inclusions, on the other hand, are formed with chemical reactions between the melt, slag and refractory. These are, in general, smaller. The biggest problem comes from hard and brittle oxide inclusions[1,2].

In the scope of this work we have focused our attention on the inclusions that are formed during the de-oxidation process with aluminium, on the modification of alumina inclusions and on the formation of spinel-type inclusions.

Steel can, after oxygen rafination, have as much as 0.1 % mass fractions of oxygen; therefore, it is essential

to have the steel deoxidized[3]. To achieve this we add different materials with a high affinity for oxygen, such as aluminium, silicon, etc. The process of de-oxidation is based on the following chemical reaction[4]:

$$x\,[\mathrm{Me}] + y\,[\mathrm{O}] = (\mathrm{Me}_x\mathrm{O}_y)^{\mathrm{slag}} \quad (1)$$

where [Me] is the dissolved metal in the liquid steel, [O] is the dissolved oxygen in the liquid steel and (Me_xO_y) is the product of the reaction, an inclusion which is reduced to slag.

Aluminium forms with oxygen alumina (Al_2O_3) inclusions, which are large, hard and brittle and are detrimental to the mechanical properties of the steel. Furthermore, they have a negative effect on the castability of the steel, because they clog the nozzles from the tundish in the continuous casting machine. With aluminium de-oxidized steel the addition of calcium modifies the alumina inclusions. The results of this reaction are calcium alumina inclusions ($CaO \cdot Al_2O_3$), which have a globular shape and their melting point is lower than the melting point of the steel[5]. They are normally larger than non-modified inclusions, however, and it is therefore essential that they are removed into the slag. Studies have shown that when we add too much calcium and the concentration of sulphur is high enough, inclusions of calcium sulphide (CaS) are formed, which also has a negative influence on the steel's castability. Thus it is important to add the correct amount of calcium to the steel, to be within the calcium concentration range, when most of the alumina inclusions are modified and the calcium content is not high enough for the CaS inclusions to form[6].

1.1 The formation of spinel phase

After de-oxidation and the formation of alumina inclusions, aluminium has a high activity as an element, because of the higher concentration in the steel and can reduce magnesium oxide from magnesite refractory and slag[7]. Magnesium forms with oxygen magnesite (MgO) inclusions. The increase in the concentration of MgO and Al_2O_3 increases the driving force for the formation of spinel-type inclusions in the calcium alumosilicate inclusion systems. Spinel-type crystals can grow almost as large as crystals of base calcium silicate.

This theory, which was suggested by Park *et al.*[8], shows the formation of spinel-type inclusions in large $CaO\text{-}SiO_2\text{-}MgO\text{-}Al_2O_3$-type inclusions with a low concentration of oxygen during the transportation of the melt from the ladle furnace to the continuous casting machine.

Another theory about the formation of spinel-type inclusions, which was suggested by Jiang *et al.*[9], shows us a different mechanism. As a result of de-oxidation alumina inclusions are formed. During the reaction between the melt, slag and refractory the magnesium is reduced from the slag or refractory:

$$2[\mathrm{Al}] + 3(\mathrm{MgO})^{\mathrm{slag\ or\ refractory}} = 3[\mathrm{Mg}] + (\mathrm{Al_2O_3}) \quad (2)$$

Before the addition of calcium for modifying the alumina inclusion, the activity of magnesium is higher than that of calcium, and therefore $MgO \cdot Al_2O_3$ and MgO inclusions are formed:

$$3[\mathrm{Mg}] + 4(\mathrm{Al_2O_3}) = 3(\mathrm{MgO} \cdot \mathrm{Al_2O_3})^{\mathrm{inclusion}} + 2[\mathrm{Al}] \quad (3)$$

$$[\mathrm{Mg}] + [\mathrm{O}] = (\mathrm{MgO})^{\mathrm{inclusion}} \quad (4)$$

After the treatment in the ladle furnace and after the addition of calcium, its activity is increased and the $CaO{\cdot}MgO \cdot Al_2O_3$ inclusions are formed:

$$4[\mathrm{Ca}] + 5(\mathrm{MgO} \cdot \mathrm{Al_2O_3})^{\mathrm{inclusion}} = 4(\mathrm{CaO} \cdot \mathrm{MgO} \cdot \mathrm{Al_2O_3})^{\mathrm{inclusion}} + [\mathrm{Mg}] \quad (5)$$

The purpose of this work was to find out which inclusions are formed in C45 steel and at what point in the steelmaking process they are formed. The study was made on C45 steel as a typical representative of the steel used for heavily stressed parts in the automobile industry.

2 EXPERIMENTAL

Samples of carbon C45 steel were taken at the company Štore Steel, d. o. o. Six samples were taken in all: the first one from the electric arc furnace, the next four from the ladle furnace and the final one from the tundish on the continuous casting machine. For the sampling we used the Sample-on-Line method or the Lollipop-Sampling method. The samples were taken at the same time as the samples for the company and they were marked from 1 to 6.

In Štore Steel, d. o. o., the chemical analysis was made on samples that were taken in parallel with our samples. Optical emission spectroscopy was used with the instrument, made by Spectro, LAVMC12A. The samples taken for further analysis were first cut, and then the smaller part was prepared for simultaneous thermal analysis (STA), while the larger part was used for the metallographic analysis, as shown in **Figure 1**. The chemical analysis of the slag was performed using a standard chemical analysis.

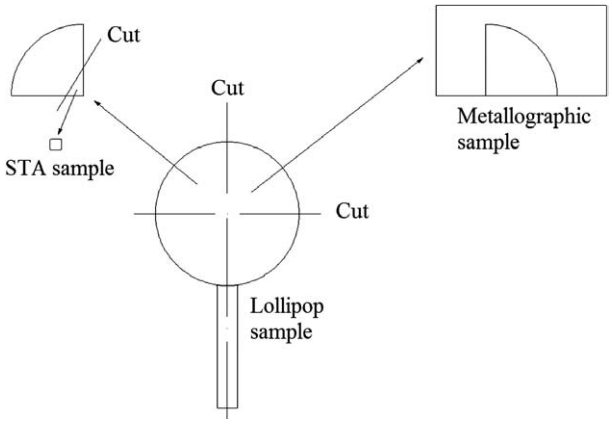

Figure 1: Cutting and preparing the samples
Slika 1: Razrez in priprava vzorcev

The characteristic temperatures were determined with a simultaneous thermal analysis (STA), which was made on a Jupiter 449c from NETSCH. For the reference an empty corundum crucible was used. The measurements were made using a dynamic argon flow.

The thermodynamic predictions were performed with Thermo-Calc TCW5 for the prediction of the solidification. The calculations were made using the TCFE3, SSUB3 and SLAG1 databases.

The metallographic analysis was made using a scanning electron microscope JEOL JSM – 5610, equipped with energy-dispersive spectroscopy (EDS). The light microscopy was made using OLYMPUS SZ61 and OLYMPUS BX61 microscopes. Finally, the micrographs were processed with the Analysis 5.0 computer program.

3 RESULTS AND DISCUSION

3.1 Chemical composition

The chemical composition of the C45 steel samples is given in **Table 1**. The chemical composition of the slag sample, which was taken at the end of ladle furnace treatment, is given in **Table 2**.

3.2 Thermodynamic calculations

The isopletic phase diagrams were predicted with Thermo-Calc. The chemical composition was taken for the calculations as shown in **Table 1**. The following elements, C, Si, Mn, Cr, Al, Mo, Ni and Fe, were taken into account; however, oxygen was not taken into account. In **Figure 2** an example of a calculated isopletic phase diagram for iron – carbon is shown, for sample 6, taken from the tundish on the continuous casting machine, with the correct carbon content marked.

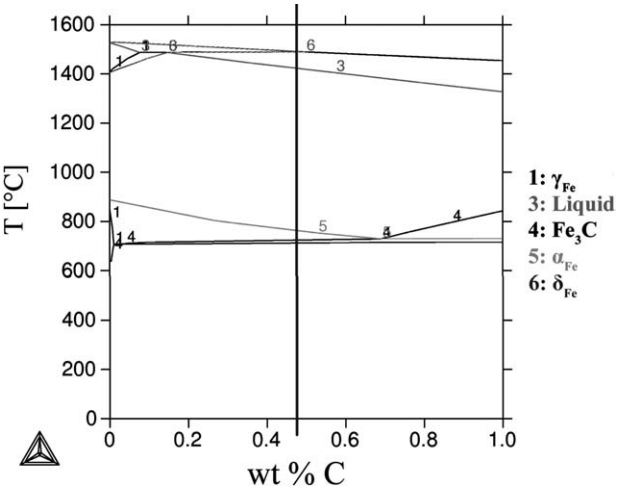

Figure 2: Isopletic phase diagram for iron–carbon for sample 6, with our carbon content marked
Slika 2: Navpični prerez faznega diagrama železo-ogljik za vzorec 6, z označeno vsebnostjo ogljika

In **Figure 3** the weight fraction of phases in dependence of the temperature is shown for sample 6, taken from the tundish on the continuous casting machine.

In **Figure 3**, in the sample taken from the tundish on the continuous casting machine, it is clear that initially a small fraction of δ-ferrite solidifies at 1490 °C, then the δ-ferrite begins its transformation into austenite at 1489 °C, and the rest of the melt begins to solidify at 1421 °C. At 761 °C the austenite begins its transformation into ferrite and later during the eutectoid phase transition into pearlite (α_{Fe} + Fe_3C). At lower temperatures the carbides precipitate from the austenitic matrix.

Table 1: Chemical composition of the C45 steel samples in mass fractions, *w*/%
Tabela 1: Kemijska sestava vzorcev jekla C45, *w*/%

Chemical element	C	Si	Mn	P	S	Cr	Mo	
Sample 1	0.13	0.03	0.13	0.011	0.036	0.11	0.04	
Sample 2	0.40	0.26	0.75	0.014	0.022	0.22	0.04	
Sample 3	0.47	0.28	0.75	0.014	0.017	0.24	0.04	
Sample 4	0.47	0.28	0.76	0.015	0.03	0.24	0.04	
Sample 5	0.47	0.27	0.75	0.014	0.027	0.24	0.04	
Sample 6	0.48	0.27	0.75	0.014	0.021	0.25	0.04	
Chemical element	Ni	Al	Cu	Sn	Ca	N	O	Fe
Sample 1	0.10	0.257	0.21	0.012	0.0004	0.007	0.0068	98.92
Sample 2	0.13	0.005	0.2	0.012	0.0004	0.008	0.0056	97.93
Sample 3	0.16	0.005	0.2	0.012	0.0005	0.008	0.0042	97.80
Sample 4	0.16	0.005	0.2	0.013	0.0003	0.007	0.0056	97.77
Sample 5	0.16	0.031	0.2	0.013	0.0003	0.008	0.0036	97.77
Sample 6	0.16	0.025	0.2	0.013	0.0001	0.008	0.0034	97.77

Table 2: Chemical composition of the slag sample
Tabela 2: Kemijska sestava vzorca žlindre

Chemical element	Si	Al	Fe	Mn	Ca	Mg	O
Content (*w*/%)	6.42	10.44	0.64	0.19	43.25	2.97	36.09

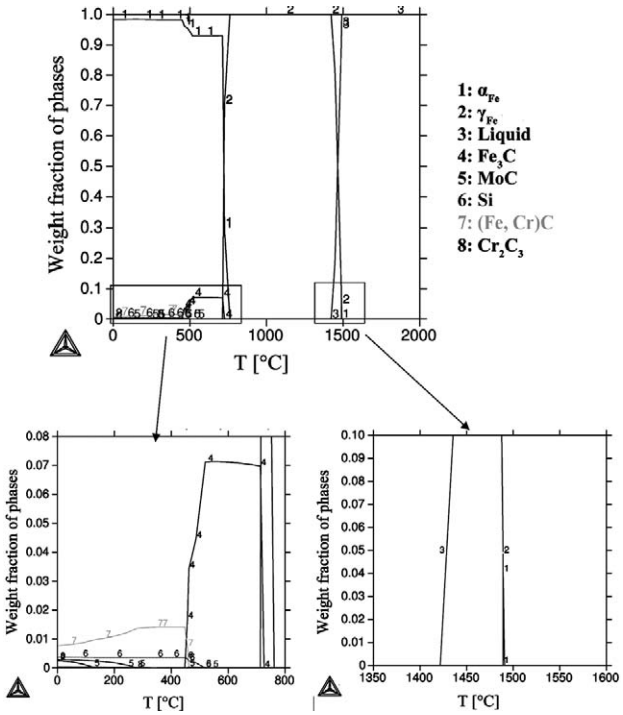

Figure 3: Weight fraction of phases in dependence of the temperature for sample 6
Slika 3: Masni delež faz v odvisnosti od temperature za vzorec 6

With Thermo-Calc it was calculated at which contents of magnesium and oxygen certain inclusions at 1550 °C are formed. Here, X represents the existence of inclusions inside the melt. The results are given in **Table 3**.

We can see that with small contents of oxygen, magnesite (MgO) inclusions are formed; with an increase of oxygen content, first the MgO inclusion and then also the spinel-type inclusions ($MgO \cdot Al_2O_3$) are formed. With the highest oxygen content the spinel-type inclusions and alumina inclusions are formed. The content of magnesium does not have an effect on the sequence of inclusion formation; it does, however, have an effect on when the inclusions are formed. At a magnesium content (in mass fractions, w) of $1 \cdot 10^{-3}$ % the first inclusions are formed at an oxygen content of $1 \cdot 10^{-5}$ %. At a magnesium content of $1 \cdot 10^{-4}$ % the first inclusions are already formed at an oxygen content of $1 \cdot 10^{-6}$ %.

With Thermo-Calc we have also analysed the slag, using the chemical composition presented in table 2. We found that at the temperatures at which the steel is in the molten state there are four different oxides in the molten or solidified state. $3CaO \cdot SiO_2$, MgO, $CaO \cdot Al_2O_3$ and $MgO \cdot Al_2O_3$ can be reduced to steel or they can first react with phases in the slag, steel, refractory or atmosphere and then be reduced to steel.

Table 3: Calculation of the possibility of inclusion formation at different contents of oxygen and magnesium
Tabela 3: Izračun možnosti nastanka vključka pri različnih vsebnostih kisika in magnezija

		Type of inclusion			Type of inclusion			
Sample 1	Content of oxygen (%)	Al(O,C)	Sample 2	Content of oxygen (%)	Spinel	MgO	Al_2O_3	mulite
Content of Mg is 0.001(%)	0.000001		Content of Mg is 0.001(%)	0.000001				
	0.00001	x		0.00001		x		
	0.0001	x		0.0001		x		
	0.001	x		0.001	x	x		
	0.0068	x		0.0056	x			x
Content of Mg is 0.0001(%)	0.000001		Content of Mg is 0.0001(%)	0.000001		x		
	0.00001	x		0.00001		x		
	0.0001	x		0.0001	x	x		
	0.001	x		0.001	x		x	
	0.0068	x		0.0056	x			x

		Type of inclusion					Type of inclusion		
Sample 5	Content of oxygen (%)	Spinel	MgO	Al_2O_3	Sample 6	Content of oxygen (%)	Spinel	MgO	Al_2O_3
Content of Mg is 0.001(%)	0.000001				Content of Mg is 0.001(%)	0.000001			
	0.00001		x			0.00001		x	
	0.0001		x			0.0001		x	
	0.001	x	x			0.001	x	x	
	0.0036	x		x		0.0036	x		x
Content of Mg is 0.0001(%)	0.000001		x		Content of Mg is 0.0001(%)	0.000001		x	
	0.00001		x			0.00001		x	
	0.0001	x	x			0.0001	x	x	
	0.001	x		x		0.001	x		x
	0.0036	x		x		0.0036	x		x

3.3 Differential scanning calorimetry

Differential scanning calorimetry was made for all the investigated samples. The rate of heating and cooling was 5 K/s. The results of the differential scanning calorimetry are DSC heating and cooling curves with determined characteristic points (solidus, liquidus) and enthalpies of fusion and solidification. We have taken a closer look at sample 6, and because it is the last sample taken from the melt it is the most representative as to which inclusions are still in the melt.

In **Figure 4** we can see a heating DSC curve for sample 6 and the process of melting. At 738.5 °C the ferrite and pearlite begin to transform to austenite. At 1401.8 °C the austenite begins to transform to δ-ferrite and to the melt, at 1509.7 °C δ-ferrite begins to melt, according to thermodynamic predictions.

In **Figure 5** we can see a cooling DSC curve for sample 6 and the process of solidifying. At 1392 °C the δ-ferrite begins to solidify and at 1383.3 °C the δ-ferrite and the melt begin to transform or solidify into austenite. At 861.8 °C the ferrite begins to segregate.

By comparing different DSC curves, we can see the difference in the characteristic temperatures and energies in more detail. In **Figure 6** is a comparison of the heating DSC curves in the temperature range from 670 °C to 850 °C, where the transformation of ferrite and pearlite to austenite occurs. The enthalpies necessary for the eutectoid phase transition are given in **Table 4**. We can see a

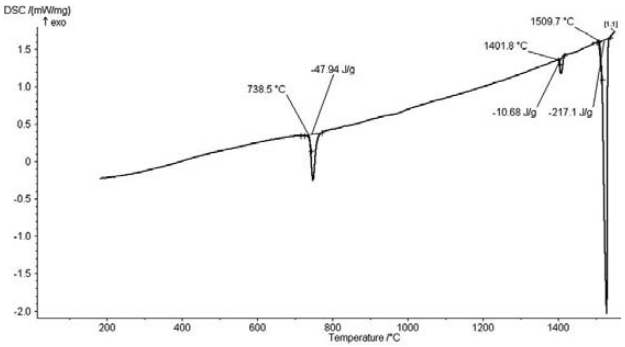

Figure 4: Heating DSC curve for sample 6
Slika 4: DSC krivulja pri segrevanju vzorca 6

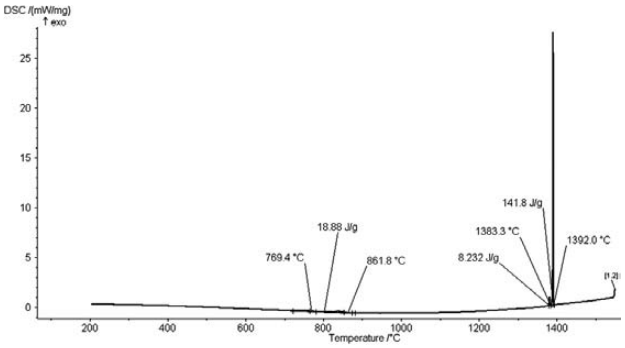

Figure 5: Cooling DSC curve for sample 6
Slika 5: DSC krivulja pri ohlajanju vzorca 6

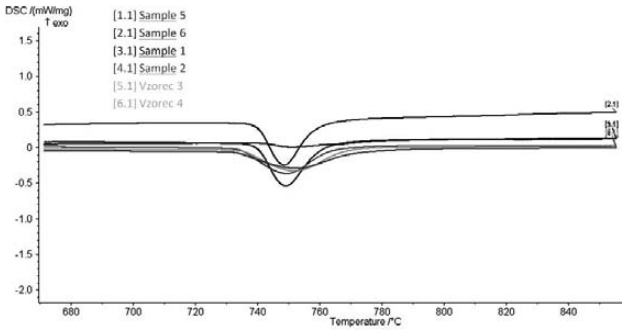

Figure 6: Enlarged comparison of the heating DSC curves for all 6 samples
Slika 6: Primerjava povečanih DSC krivulj segrevanja vseh 6 vzorcev

significant difference in sample 1; this is due to the fact that the eutectoid reaction is presented in a small manner. After the treatment on the ladle furnace the enthalpy is higher.

Table 4: The enthalpy necessary for eutectoid phase transition
Tabela 4: Entalpija, potrebna za eutektoidno fazno premeno

Sample	1	2	3	4	5	6
Energy (J/g)	3.18	35.29	38.61	38.16	47.38	47.94

In **Figure 7** we can see a comparison of the DSC curves in the temperature range from 530 °C to 1020 °C or during the eutectoid phase transition. In **Table 5** the enthalpies during the eutectoid phase transition are given. We can see a major difference between the samples 2 and 4 and the rest of the samples. This can be explained by the fact that with samples 2 and 4 the eutectoid phase transition occurs at a lower temperature than with the other samples and a certain part of the energy released is related to the magnetic phase transition, resulting in the determined enthalpy values.

Table 5: The enthalpy during the eutectoid phase transition
Tabela 5: Entalpija pri eutektoidni fazni premeni

Sample	1	2	3	4	5	6
Energy (J/g)	22.67	65.93	35.9	63.29	28.73	18.88

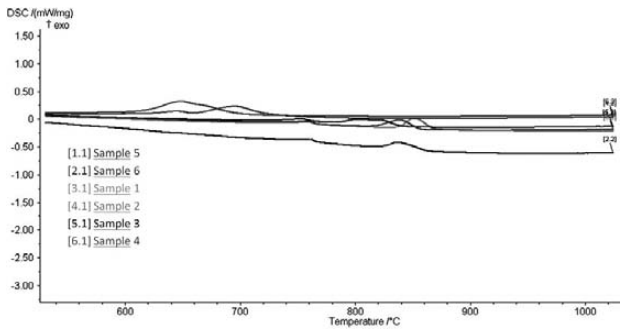

Figure 7: Enlarged comparison of the cooling DSC curves for all 6 samples
Slika 7: Primerjava povečanih DSC krivulj ohlajanja, za vseh 6 vzorcev

In general we can see that the heating DSC curves relate well to the microstructure of our samples. The calculated enthalpies necessary for the eutectoid phase transition and the calculated fraction of microstructural phases have a high correlation; this is a result of the fast cooling of the industrial samples. The cooling DSC curves, on the other hand, have a much better correlation with the phase diagrams calculated with Thermo-Calc because of a steady cooling rate.

3.4 Microstructure analysis

The microstructure of our samples can be seen in **Figure 8**. It has, with the exception of sample 1, a small fraction of ferrite (α_{Fe}) and a large fraction of pearlite (α_{Fe} + Fe_3C). Sample 1 has a small fraction of pearlite (α_{Fe} + Fe_3C) and a large fraction of ferrite (α_{Fe}). The precise fractions of the microstructural phases are shown in **Table 6**. These fractions were calculated at 200-times magnification.

Table 6: Fraction of microstructural phases for all samples.
Tabela 6: Delež faz v mikrostrukturi vseh vzorcev

Sample	1	2	3	4	5	6
Ferrite (%)	77.1	7.1	3.2	4.7	1.9	2.2
Pearlite (%)	22.9	92.9	96.8	95.3	98.1	97.8

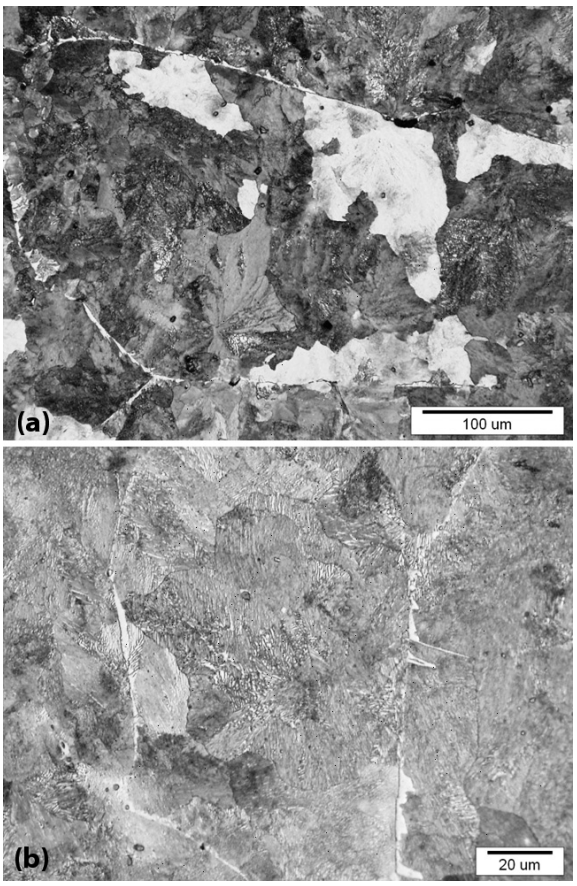

Figure 8: Microstructure: ferrite and pearlite; a) sample 5, b) sample 6
Slika 8: Mikrostruktura: ferit in perlit; a) vzorec 5, b) vzorec 6

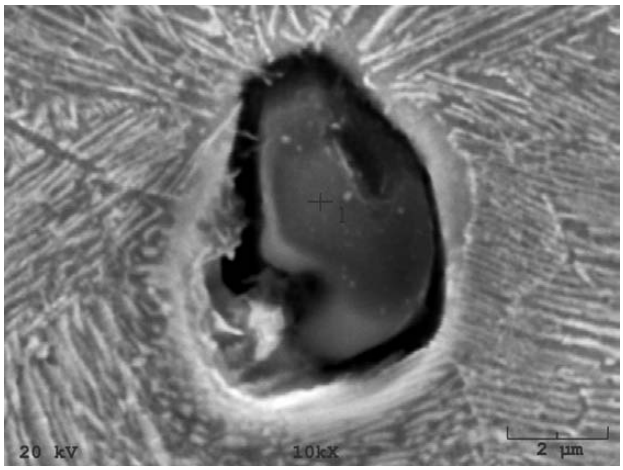

Figure 9: Alumina inclusion (Al_2O_3) and the place of the point analysis determined in sample 6
Slika 9: Vključki Al_2O_3 in mesto točkaste analize na vzorcu 6

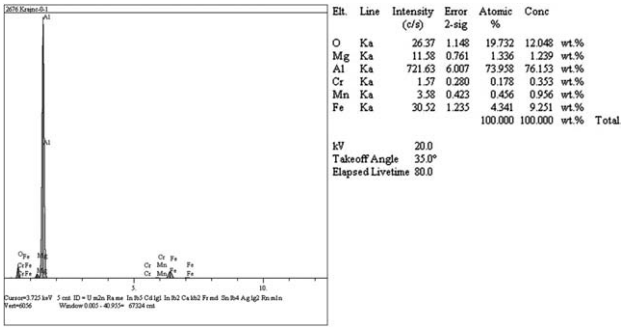

Figure 10: The result of the point analysis of an alumina inclusion
Slika 10: Rezultati točkaste analize vključka Al_2O_3

In **Figure 8** the microstructures of sample 5 and 6 can be seen. There is a large fraction of pearlite (α_{Fe} + Fe_3C) and small fraction of ferrite (α_{Fe}) on the austenite phase boundaries.

With the scanning electron microscope we found different types of inclusions in our samples: Al_2O_3, MnS and spinel-type ($MgO \cdot Al_2O_3$) modified with calcium. We made a point and mapping analysis. In **Figure 9** we can see an alumina inclusion in sample 6. The results of the EDS analysis of the alumina inclusion are presented in **Figure 10**.

In the sample 6 microstructure there are also MnS inclusions. Similar inclusions where found by Lamut *et al.*[10] in a sample taken from the tundish on a continuous casting machine. The EDS analysis of this inclusion is shown in **Figure 11**. In our sample taken from tundish some magnesite and alumina inclusions were also found, but they were small and usually not larger than 1 µm.

In **Figure 12** a spinel-type ($MgO \cdot Al_2O_3$) inclusion modified with calcium is shown. It was found in sample 5 and its chemical composition is determined with a mapping analysis, also shown in **Figure 12**.

The inclusion found in sample 5 is a product of the de-oxidation process with aluminium, during which

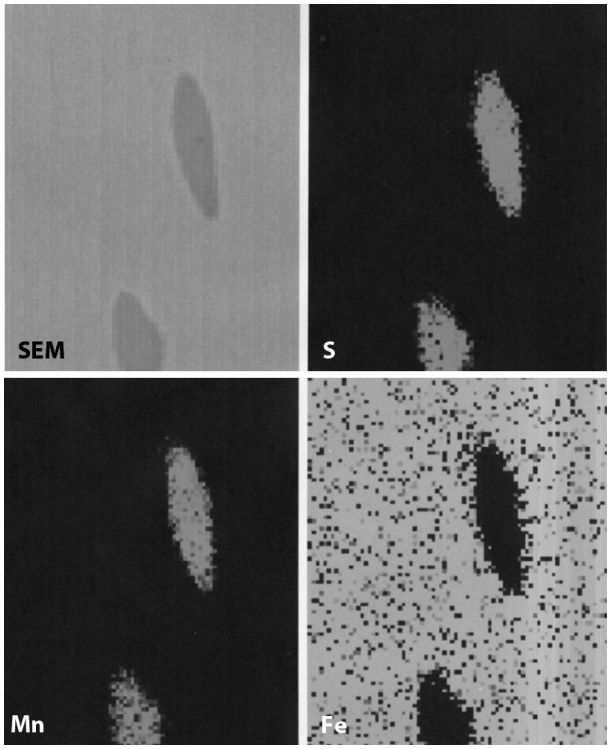

Figure 11: Microstructure and mapping analysis of MnS[10]
Slika 11: Mikrostruktura in razporeditev elementov v MnS[10]

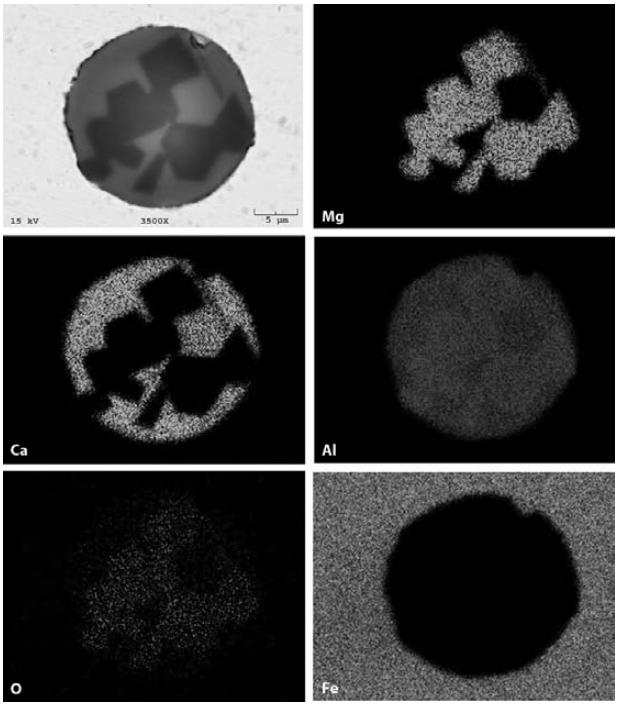

Figure 12: Mapping analysis of the spinel-type inclusion modified with calcium
Slika 12: Razporeditev elementov v vključku špinela, modificiranega s kalcijem

alumina inclusions were formed. We assume that because of the high content of aluminium in the melt, it has reduced the magnesium from the refractory and the slag. The magnesium then reacted with the oxygen and magnesite inclusions were formed. These have then, because of the high content, reacted with alumina and spinel-type inclusions were formed. With the addition of calcium for modifying the inclusions, there was a reaction between the spinel-type inclusions and pure alumina with calcium. The result of this was a large globural CaO-MgO-Al_2O_3 system inclusion.

In agreement with the literature[7] alumina inclusions are created during the de-oxidation process with aluminium. Furthermore, in accordance with Jiang *et al.*[9], the aluminium content in the melt is increased and it reduces the magnesium. Magnesium in turn, according to Park *et al.*[8], because of the high activity, reacts with the remaining oxygen, and forms magnesite inclusions, which then react with alumina and spinel-type inclusions are formed[7]. Because there are more alumina inclusions, some of them are trapped in the matrix of the spinel-type inclusion and these are, with the addition of calcium in accordance with Pires *et al.*[6], modified into large globular inclusions[5]. The EDS analysis verifies this theory, as we see in **Figure 11** that there is an angular phase formed from MgO and Al_2O_3 in the middle of the inclusion, while there is a CaO and Al_2O_3 phase surrounding the first one and making the inclusion globular.

4 CONCLUSIONS

Based on an analysis of the C45 steel sample, the following conclusions can be drawn:

The thermodynamic calculation has shown that for low contents of oxygen in the melt, initially magnesite inclusions are formed, and with an increase in the oxygen content magnesite and spinel-type inclusion are formed, whereas at high oxygen contents spinel-type and alumina inclusions are formed.

The thermodynamic calculation of the phase equilibrium revealed that the formation of $3{\cdot}CaO \cdot SiO_2$, MgO, $CaO \cdot Al_2O_3$ and $MgO \cdot Al_2O_3$ oxides in the slag is possible. These can react with phases in the slag, steel, refractory or atmosphere and can be reduced to steel.

With the calculation of the thermodynamic equilibrium we found that the magnesite, alumina and spinel-type inclusion are formed during the ladle furnace treatment. The EDS analysis confirmed that at the end of the ladle furnace treatment there are spinel-type inclusions in the melt and that they are modified with calcium. There is a possibility that the inclusions are removed during the manipulation from the ladle furnace to the continuous casting machine, because no large oxide inclusion was found in our tundish sample. Small alumina inclusions (1 µm) were found as were small MnS inclusions.

5 REFERENCES

[1] Y. Payandeh, M. Soltanieh, Oxide Inclusions at Different Steps of Steel Production, Journal of Iron and Steel Research, International, 14 (**2007**) 5, 39–46

[2] H. V. Atkinson, G. Shi, Characterization of Inclusions in Clean Steel: a Review Including the Statistics of Extreme Methods, Progress in Materials Science, 48 (**2003**), 457–520

[3] V. Gontarev, Teorija metalurških procesov. Univerza v Ljubljani, Naravoslovnotehniška fakulteta, Oddelek za materiale in metalurgijo. Ljubljana, 2005, 129

[4] A. Ghosh, Secondary Steelmaking: Principles and Aplication. Library of Congress Cataloging-in-Publication Data, 2000, 672

[5] F. Tehovnik, B. Koroušić, V. Prešeren, Optimizacija modifikacije nekovinskih vključkov v jeklih obdelanih s Ca, Kovine Zlitine Tehnol., 26 (**1992**) 1/2, 125–130

[6] J. C. S. Pires, A. Garcia, Modification of Oxide Inclusions Present in Aluminum-Killed Low Carbon Steel by Addition of Calcium. REM: R. Esc. Minas, Ouro Preto, 57 (**2004**) 3, 183–189

[7] D. Steiner Petrovič, B. Arh, F. Tehovnik, M. Pirnat, Magnesium Non-metallic Inclusions in Non-Oriented Electrical Steel Sheets, ISIJ International, 51 (**2010**) 12, 2069–2075

[8] J. H. Park, Formation Mechanism of Spinel-Type Inclusions in High-Alloyed Stainless Steel Melts, The Minerals, Metals & Materials Society and ASM International, 38B (**2007**), 657–663

[9] M. Jiang, X. Wang, B. Chen, W. Wang, Laboratory Study on Evolution Mechanisms of Non-metallic Inclusions in High Strength Alloyed Steel Refined by High Basicity Slag, ISIJ International, 50 (**2010**) 1, 95–104

[10] J. Lamut, M. Knap, H. Ploštajner, B. Senčič, Proces modifikacije vključkov s CaSi, 13. Seminar o procesni metalurgiji jekla, 2007, 134–137